Oxygenated Biofuels from Butanol for Diesel Blends: Synthesis of the Acetal 1,1-Dibutoxyethane Catalyzed by Amberlyst-15 Ion-Exchange Resin

Nuno S. Graça,[†] Luís S. Pais,[‡] Viviana M. T. M. Silva,[†] and Alírio E. Rodrigues*,[†]

Laboratory of Separation and Reaction Engineering (LSRE), Department of Chemical Engineering, Faculty of Engineering, University of Porto, Rua Dr. Roberto Frias s/n, 4200-465 Porto, Portugal, and School of Technology and Management, Bragança Polytechnic Institute, Campus de Santa Apolónia, Apartado 1134, 5301-857 Bragança, Portugal

The synthesis of 1,1-dibutoxyethane or acetaldehyde dibutylacetal was studied in a batch reactor by reacting butanol and acetaldehyde in a liquid phase, using Amberlyst-15 as the catalyst. The reaction equilibrium constant was experimentally determined in the temperature range 20−40 °C at 6 atm, where $K_a = 0.00959 \exp[1755.3/T\ (\mathrm{K})]$. The standard properties of the reaction at 298.15 K were estimated: $\Delta H° = -14.59$ kJ mol^{-1}, $\Delta G° = -3.07$ kJ mol^{-1}, and $\Delta S° = -38.64$ J mol^{-1} K^{-1}. Kinetic experiments were performed in the temperature range 10−50 °C at 6 atm. A two-parameter kinetic law based on a Langmuir−Hinshelwood rate expression, using activity coefficients from the UNIFAC method, was used. The kinetic parameters are $k_c = 2.39 \times 10^9 \exp[-6200.9/T\ (\mathrm{K})]$ (mol g_{cat}^{-1} min^{-1}) and $k_{s,D} = 2.25 \times 10^{-4} \exp[3303.1/T\ (\mathrm{K})]$. The activation energy of the reaction is 51.55 kJ mol^{-1}. This work is an important step for further implementation of an integrated reaction−separation process, such as a simulated moving-bed reactor.

1. Introduction

In the last years, there has been a growing interest in the development of environmentally friendly gasoline and diesel fuels. Oxygenated additives can be used in order to reduce HC and CO emissions and provide a high octane quality of unleaded gasoline.[1] The increase of the oxygen content in diesel fuel reduces significantly the particulate levels; studies showed that the Bosh smoke number (a measure of the particulate or soot levels in diesel exhaust) falls from about 55% for conventional diesel fuel to less than 1% when the oxygen content of the fuel is above about 25% by mass.[2] Methyl and ethyl *tert*-butyl ether (MTBE and ETBE, respectively) are widely used as gasoline additives, providing enhancement of the octane number and a significant reduction of tailpipe pollution. However, these ethers are not suitable as diesel oxygenates because they drastically reduce the cetane number in diesel blends; for example, the ETBE cetane number is 2.5,[3] with the minimum value being 51, according to directive 2003/17/EC. Acetals have been under consideration as oxygenated additives to diesel fuel.[4] The use of the acetal 1,1-diethoxyethane as a diesel fuel additive has shown a marked reduction of exhaust smoke.[5] Moreover, acetals are useful as raw materials for perfumes, agricultural chemicals, and pharmaceuticals;[6] they also can be used in the flavoring of food, in the design of synthetic perfumes,[7,8] as a mineral oil substitute,[9] in the production of poly(vinylic ether)s, and as an intermediate in condensation reactions.[10,11]

Acetals can be produced by the acid-catalyzed addition of 2 mol of monohydric alcohol and 1 mol of aldehyde.[12] There is a particular interest in the use of ethanol and acetaldehyde as reactants because they are subproducts of the cane sugar industry, and therefore DEE or acetaldehyde diethylacetal can be produced by means of natural resources.[13] Recently, butanol has been considered as an alternative to ethanol as a biofuel.[14] Butanol has several advantages over ethanol, such as higher energy content, lower water absorption, better blending ability, and use in conventional combustion engines without modifications. Therefore, butanol is also a possible bioderivable reactant to produce the acetal DBE or acetaldehyde dibutylacetal.

The synthesis of acetals is typically carried out under conditions of homogeneous catalysis;[15] however, the use of strong liquid inorganic acids like H_2SO_4, HCl, and HI as the catalyst brings some disadvantages, namely, separation problems due to miscibility with a reaction medium and equipment corrosion at a high catalyst concentration.[16,17] Therefore, heterogeneous catalysts, such as ion-exchange resins and zeolites,[18,19] become a safer alternative for acetal production. Previous works report the use of heterogeneous catalysts for synthesis of the acetal 1,1-diethoxyethane using Amberlyst-15 and -18[13,20] and the acetal 1,1-dimethoxyethane using Amberlyst-15, a Y-type zeolite, and SMOPEX 101 fibres.[21,22]

Amberlyst-15 proved to be an efficient catalyst for acetalization of butanol with heptanal[23] and formaldehyde;[24] however, it was verified that side reactions are influenced by the type of ion-exchange resins in the esterification of *n*-butanol with acetic acid at 100−120 °C. The observed side reaction products using Purolite CT 269 (monosulfonated) and Amberlyst-48 (bisulfonated) were isomers of butene, di-*n*-butyl ether, and *sec*-butyl-*n*-butyl ether as well as *sec*-butanol and *sec*-butyl acetate, whereas with Amberlyst-46 (surface-sulfonated), side reactions were almost negligible.[25]

In this work, synthesis of the acetal 1,1-dibutoxyethane (DBE) from butanol and acetaldehyde by means of a liquid-phase reaction catalyzed by Amberlyst-15 is studied in order to obtain thermodynamic and kinetic data for further implementation of the integrated reaction−separation processes of fixed-bed reactors and simulated moving bed reactors (SMBRs). Because the reaction is equilibrium-limited, the use of an integrated reaction−separation process, such as a SMBR, allows the displacement of chemical equilibrium toward product formation.[20,26]

* To whom correspondence should be addressed. Tel.: +351225081671. Fax: +351225081674. E-mail: arodrig@fe.up.pt.
[†] University of Porto.
[‡] Bragança Polytechnic Institute.

10.1021/ie901635j
Published on Web 04/08/2010

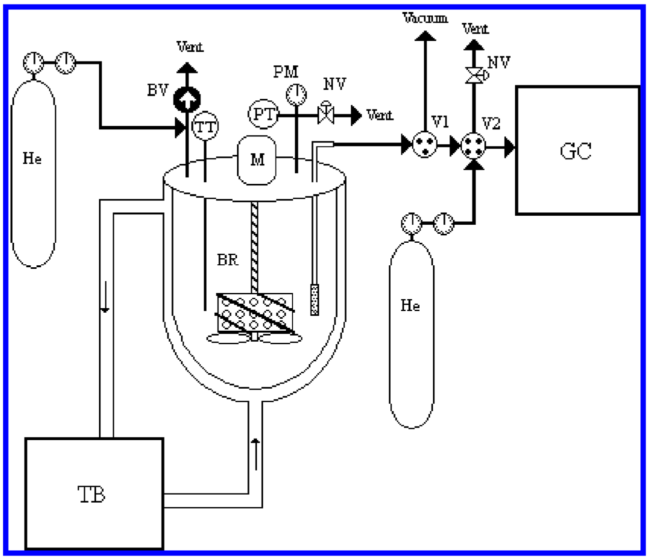

Figure 1. Experimental setup for kinetic studies: BR, batch reactor; M, motor; TT, temperature sensor; PT, pressure sensor; PM, manometer; BV, blow-off valve; V1, sampling valve; V2, injection valve; NV, needle valve; GC, gas chromatograph; TB, thermostati bath.

2. Experimental Section

2.1. Reactor. The experiments were carried out in a glass-jacketed 1 dm^3 autoclave (Büchi, Flawil, Switzerland), operating in a batch mode, mechanically stirred, equipped with pressure and temperature sensors and with a blow-off valve. The temperature was controlled by thermostatted water (Lauda, Lauda-Königshofen, Germany) that flows through the jacket. To maintain the reacting mixture in the liquid phase over the whole temperature range, the reactor was pressurized with helium. Figure 1 shows a schematic representation of the experimental setup. A dry catalyst is placed in a basket at the top of the stirrer shaft and falls down in the reactant solution at the beginning of agitation; therefore, the time zero for the reaction is well-defined. One of the outlets of the reactor was connected to the liquid sampling valve (Valco, Houston, TX), which injects 0.1 μL of pressurized liquid into a gas chromatograph.

2.2. Catalyst. The catalyst used was the ion-exchange resin Amberlyst-15 (Rohm and Haas, Philadelphia, PA). The ion-exchange capacity is 4.7 mequiv $g_{\text{dry resin}}^{-1}$, and the surface area is 53 $m^2\ g^{-1}$.

2.3. Chemicals. The reactants used were butanol (>99.9% pure) and acetaldehyde (>99.5% pure) (Sigma-Aldrich, Madison, WI).

2.4. Analytical Method. The samples were analyzed on a gas chromatograph (Chrompack 9100; Varian, Palo Alto, CA), and the compounds were separated in a fused-silica capillary column (Chrompack CP-Wax 57 CB), 25 m × 0.53 mm i.d., and df = 22.0 μm using a thermal conductivity detector (TCD 903 A) for peak detection. The column temperature was programmed with a 5 min initial hold at 75 °C, followed by a 25 °C min^{-1} ramp up to 100 °C, where it was held for 1.5 min. The temperature of the injector was set at 150 °C. The carrier gas used was Helium N50.

3. Thermodynamic Equilibrium Constant

DBE and water are produced by the acid-catalyzed addition of 2 mol of butanol and 1 mol of acetaldehyde:

$$\text{2butanol (A)} + \text{acetaldehyde (B)} \Leftrightarrow \text{DBE (C)} + \text{water (D)}$$

Table 1. Experimental Equilibrium Compositions and Equilibrium Constants[a]

	T (K)			
	293.15	303.15	313.15	323.15
x_A	0.40720	0.42078	0.43979	0.45274
x_B	0.16090	0.16742	0.17362	0.17915
x_C	0.21595	0.20590	0.19330	0.18406
x_D	0.21595	0.20590	0.19330	0.18406
K_x	1.74794	1.43165	1.11269	0.92256
γ_A	1.07895	1.08250	1.08363	1.08343
γ_B	1.14948	1.14763	1.14400	1.14096
γ_C	1.38198	1.38971	1.40227	1.40939
γ_D	2.11094	2.16536	2.21667	2.27337
K_γ	2.17916	2.23767	2.31391	2.39235
$K_a = K_x K_\gamma$	3.80905	3.20023	2.57467	2.20709

[a] Experimental conditions: w_{cat} = 1.8 g, V = 530 mL, P = 6 atm, $r_{A/B}$ = 2.2, and 0.5 mm < d_p < 0.6 mm.

The equilibrium constants based on activities[27] as shown in eq 1 were calculated for different temperatures (in the range of 293.15−323.15 K), at 6 atm, at a stoichiometric initial molar ratio of reactants butanol/acetaldehyde ($r_{A/B}$ = 2.2); the total volume of the reactants was 530 mL and the mass of the catalyst 1.8 g. It was ensured that, for these conditions, the amounts of adsorbed species are negligible, and there was only one liquid phase in spite of the fact that water and *n*-butanol are only partially miscible; therefore, the equilibrium composition is only related to the thermodynamic reaction equilibrium. Moreover, it was not detected any byproduct. The equilibrium constants were calculated from the experimentally measured equilibrium composition and activity coefficients of the species (γ_i) calculated by the UNIFAC method (Table 1).[28] The parameters used are presented in Appendix A.

$$K_a = \frac{a_C a_D}{a_A^2 a_B} = \frac{x_C x_D}{x_A^2 x_B}\frac{\gamma_C \gamma_D}{\gamma_A^2 \gamma_B} = K_X K_\gamma \tag{1}$$

At equilibrium, the standard free-energy change is related to the equilibrium constant by

$$\Delta G° = -RT \ln K_a \tag{2}$$

By definition, the standard free-energy change is related to standard enthalpy and entropy changes by

$$\Delta G° = \Delta H° - T\Delta S° \tag{3}$$

Therefore, temperature dependence of the equilibrium constant is given by

$$\ln K_a = \frac{\Delta S°}{R} - \frac{\Delta H°}{R}\frac{1}{T} \tag{4}$$

The standard free energy, enthalpy, and entropy changes for this reaction can be estimated by fitting experimental values of ln K_{eq} vs 1/T (Figure 2). From the slope, it is concluded that the reaction is slightly exothermic with $\Delta H°$ = −14 593.6 J mol^{-1}, and from the intercept, $\Delta S°$ = −38.6 J mol^{-1} K^{-1} and $\Delta G°$ = −3074.1 J mol^{-1} calculated from eq 3.

4. Kinetic Results

The influence of the external mass-transfer resistance was studied by performing experiments at different stirring speeds. The external mass-transfer resistance is eliminated for a stirring speed above 800 rpm. Therefore, all further experiments were carried out at 800 rpm.

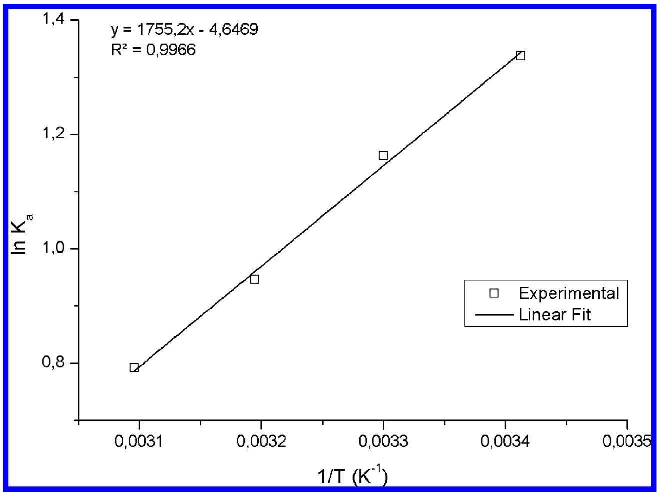

Figure 2. Linearization of the experimental equilibrium constants.

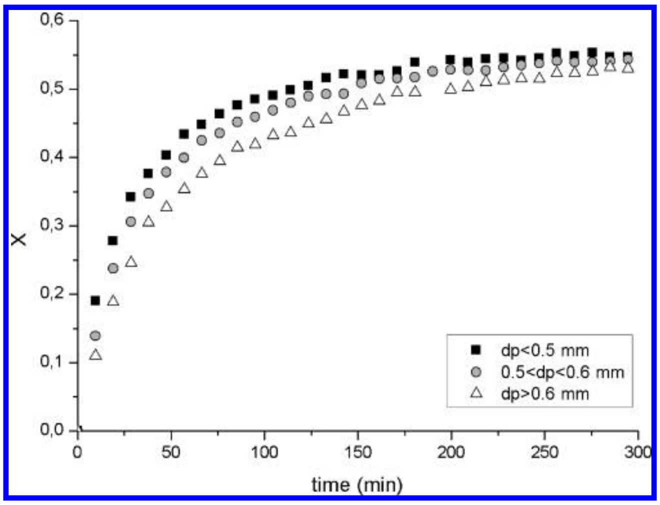

Figure 3. Effect of the particle size on the conversion of the acetaldehyde history: T = 293.15 K, P = 6 atm, $r_{A/B}$ = 2.2, w_{cat} = 1.8 g, and V = 530 mL.

4.1. Effect of the Particle Size. Determination of the concentration of acidic sites of Amberlyst-15 resin for different particle diameters[29] shows that the concentration of acid sites is independent of the particle size; therefore, any difference in reaction kinetics for different particle sizes can only be attributed to the internal mass-transfer resistance.

Experiments carried out with different particle sizes of the catalyst show internal diffusion limitations for experiments with particle diameters greater than 0.5 mm (Figure 3). For diameters of particles below 0.5 mm, it is not possible make conclusions about internal diffusion limitations. Therefore, the kinetic parameters will be estimated by using a detailed model accounting for intraparticle diffusion.

4.2. Mass of the Catalyst Effect. The conversion increases with an increase in the mass of the catalyst (Figure 4) for the same experimental conditions.

The maximum reaction rate occurs at the beginning of the reaction, where the slope of the plot conversion versus time is higher. The initial slopes for catalyst masses of 1.8 and 3.0 g are 0.0176 and 0.0296, respectively. The ratio between the catalyst mass is 3.0/1.8 = 1.67, and the ratio between the initial slopes is 0.0296/0.0176 = 1.68. These results show that the initial reaction rate increased in the same proportion as the mass of the catalyst.

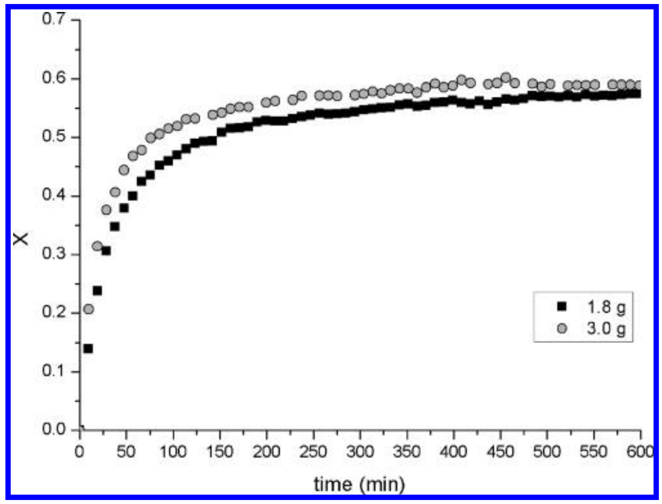

Figure 4. Effect of the mass of the catalyst on the conversion of the acetaldehyde history: T = 293.15 K, P = 6 atm, $r_{A/B}$ = 2.2, V = 530 mL, and 0.5 mm < d_p < 0.6 mm.

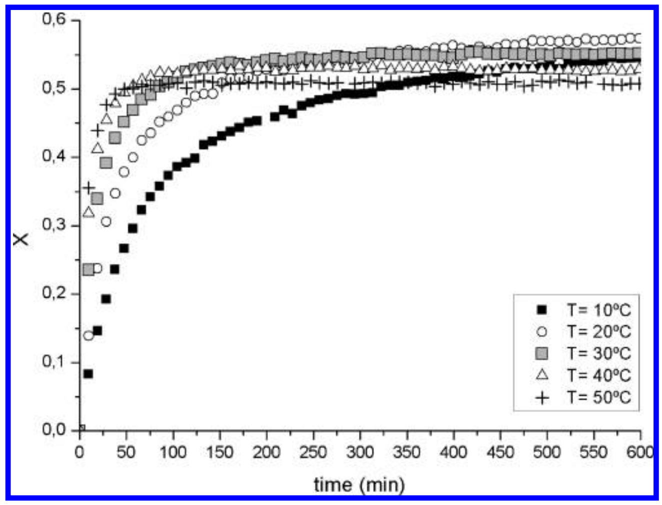

Figure 5. Effect of the temperature on the conversion of the acetaldehyde history: P = 6 atm, $r_{A/B}$ = 2.2, w_{cat} = 1.8 g, V = 530 mL, and 0.5 mm < d_p < 0.6 mm.

4.3. Effect of the Temperature. Experiments performed at different temperatures show that the rate of reaction increases with the temperature; however, the equilibrium conversion of acetaldehyde decreases because of the exothermic nature of the reaction (Figure 5). For batch or fixed-bed reactors, this could be an issue because the conversion decays from about 57% at 20 °C to about 48% at 50 °C. However, from the perspective of process intensification by means of a reactive separation such as the SMBR technology, it is more important to enhance the kinetics of the reaction because equilibrium is displaced by product removal, with complete depletion of the reactants being possible to achieve. At higher temperatures, the mixture viscosity decreases, benefiting also the mass-transfer mechanisms and reducing pressure drops in the bed. Moreover, for multicomponent adsorption equilibria, the effect of the temperature on the selectivity of the resin will play a critical role. For ethyl lactate synthesis, the selectivity of water/ethyl lactate decreases by a factor of 3.5 (from 86.7 to 24.8) when the temperature is increased from 20 to 50 °C.[30]

4.4. Effect of the Initial Molar Ratio of the Reactants. It is known that one way of increasing the conversion is to use an excess of one reactant, in order to shift the equilibrium toward product formation. However, when the catalyst productivity is

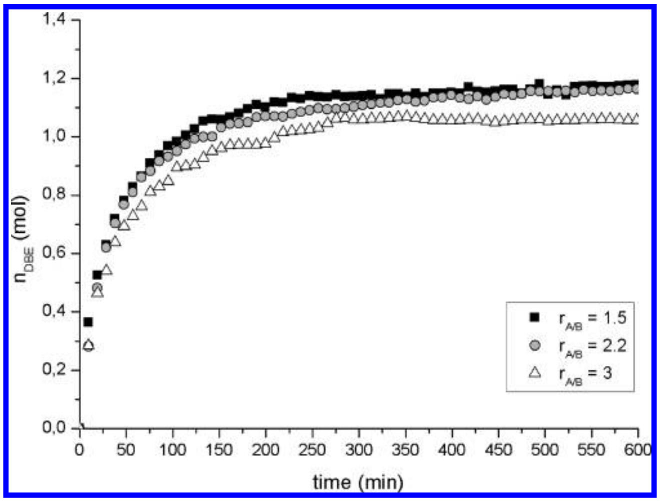

Figure 6. Effect of the initial molar ratio of the reactants on the number of moles of the DBE history: $T = 293.15$ K, $P = 6$ atm, $w_{cat} = 1.8$ g, $V = 530$ mL, and 0.5 mm < d_p < 0.6 mm.

analyzed for the same catalyst loading (mass of the resin per volume of reactants), the maximum quantity of DBE is achieved for the stoichiometric ratio of the reactants ($r_{A/B} = 2$), as shown in Figure 6. Moreover, the initial molar ratio ($r_{A/B}$) does not significantly affect the rate of the reaction; therefore, there is no need to operate at a molar ratio of the reactants far from the stoichiometric one.

5. Batch Reactor Model

As shown in Figure 3 for particle diameters greater than 0.5 mm, the kinetics of the reaction is affected by internal mass-transfer resistances; for smaller diameter particles, it is not possible to conclude about internal mass-transfer resistances. Therefore, an isothermally operated batch reactor model that considers diffusion of the components inside the catalyst particle will be used.[20] In this work, surface diffusion was neglected; however, Dogu et al.[31] showed that although molecular diffusion is the main transport mechanism in macropores, surface diffusion could also have a significant contribution. From our knowledge, this behavior was not reported or noticed for esterification or acetalization reactions. Therefore, surface diffusion was not considered in this work.

Mass balance in the bulk fluid:

$$\frac{\mathrm{d}C_{b,j}}{\mathrm{d}t} = -\frac{A_p}{V_{liq}} D_j \left.\frac{\partial C_{p,j}}{\partial r}\right|_{r=r_p} \quad (j = \mathrm{A{-}D}) \tag{5}$$

with

$$A_p = \frac{3}{r_p} V_p \tag{6}$$

where $C_{b,j}$ is the bulk concentration of component j, $C_{p,j}$ is the concentration of component j inside the particle pores, A_p is the external area between the fluid and particle, V_{liq} is the volume of liquid inside the reactor, D_j is the effective diffusivity of component j inside the particle pores (Appendix B), r_p is the particle radius, V_p is the total volume of particles,r is the particle radial position, and t is the time coordinate.

Mass balance in the particle:

$$\varepsilon_p \frac{\partial C_{p,j}}{\partial t} = \frac{1}{r^2}\frac{\partial}{\partial r}\left[D_j r^2 \frac{\partial C_{p,j}}{\partial r}\right] + (1 - \varepsilon_p) \upsilon_j \rho_s \mathscr{R}^p \tag{7}$$

where ε_p is the particle porosity, υ_j is the stoichiometric coefficient of the component j, ρ_s is the true density of the resin, and $\mathscr{R}^p$ is the reaction rate relative to the local concentration (in mol g_{cat}^{-1} min^{-1}).

Initial conditions:

$$t = 0, \quad C_{b,j} = C_{b0,j}; \quad C_{p,j} = C_{p0,j} \tag{8}$$

Considering the external mass-transfer resistance as negligible, the boundary conditions are

$$r = 0, \quad \frac{\partial C_{p,j}}{\partial r} = 0 \tag{9}$$

$$r = r_p, \quad C_{b,j} = C_{p,j}|_{r=r_p} \tag{10}$$

Upon introduction of the dimensionless space variable $\rho = r/r_p$, the model equations become

$$\frac{\mathrm{d}C_{b,j}}{\mathrm{d}t} = -\frac{3}{r_p^2}\frac{1 - \varepsilon_b}{\varepsilon_b} D_j \left.\frac{\partial C_{p,j}}{\partial \rho}\right|_{\rho=1} \tag{11}$$

where ε_b is the bulk porosity.

$$\frac{\partial C_{p,j}}{\partial t} = \frac{D_j}{r_p^2}\frac{1}{\rho^2}\frac{\partial}{\partial \rho}\left[\rho^2 \frac{\partial C_{p,j}}{\partial \rho}\right] + \frac{1 - \varepsilon_p}{\varepsilon_p} \upsilon_j \rho_s \mathscr{R}^p \tag{12}$$

Boundary conditions:

$$\rho = 0, \quad \frac{\partial C_{p,j}}{\partial \rho} = 0 \tag{13}$$

$$\rho = 1, \quad C_{p,j} = C_{p,j}|_{\rho=1} \tag{14}$$

5.1. Kinetic Model. In this work, the Langmuir–Hinshelwood model equation (15) was considered, following previous experience in our laboratory with diethylacetal and dimethylacetal synthesis.[13,21] The reaction rate is

$$\mathscr{R} = k_c \frac{a_A a_B - \dfrac{a_C a_D}{K_a a_A}}{\left(1 + K_{s,A} a_A + K_{s,B} a_B + K_{I_1} a_A a_B + K_{I_2} \dfrac{a_C}{a_A} + K_{s,C} a_C + K_{s,D} a_C + K_{s,D} a_D\right)^2} \tag{15}$$

This model is based on adsorption of the reactant species (butanol and acetaldehyde), the reaction between adsorbed reactants on the catalyst surface, and desorption of the reaction products (water and DBE). The surface reaction involves three steps:

Surface reaction between the adsorbed species of butanol (A) and acetaldehyde (B) to give adsorbed hemiacetal, I_1S:

$$\mathrm{AS} + \mathrm{BS} \overset{K_1}{\Leftrightarrow} \mathrm{I_1S} + \mathrm{S}$$

Table 2. Estimated Model Parameters

	T (K)		
	293.15	303.15	313.15
k_c (mol g^{-1} min)	1.5761	3.0424	6.091
$K_{s,D}$	16.765	12.338	8.649

Surface reaction to obtain adsorbed water, DS:

$$I_1S + S \overset{K_2}{\Leftrightarrow} I_2S + DS$$

Surface reaction to obtain adsorbed acetal, CS:

$$I_2S + AS \overset{K_3}{\Leftrightarrow} CS + S$$

The reaction where water is formed (step 2) was assumed to be the rate-controlling step because formation of the intermediate I_2 from the protonated hemiacetal is the rate-determining step for acetalization.[32,33] Because of the acidic property of Amberlyst-15, water will be the more adsorbed component; therefore, when the other adsorption constants are neglected, the kinetic model can be reduced to a three-parameter equation (eq 16):

$$\mathscr{R} = k_c \frac{a_A a_B - \dfrac{a_c a_D}{K_a a_A}}{(1 + K_{s,D} a_D)^2} \qquad (16)$$

6. Numerical Solution

The model equations were solved using the commercial software *gPROMS* (general PROcess Modeling System), version 3.1.5. The batch reactor model is defined by a set of partial differential equations. The radial domain was discretized using the second-order orthogonal collocation in the finite-element method (OCFEM). The system of ordinary differential equations, resulting from radial discretization, was integrated over time using DASOLV integrator implementation in *gPROMS*. For radial discretization, 10 finite elements with two collocation points were used in each element. For all simulations, a tolerance equal to 10^{-5} was fixed.

6.1. Parameter Estimation. In order to determine the parameters of the reaction rate model proposed, it is necessary to find a combination of these parameters that provide the best fit of the batch reactor model results with experimental measurements.

The parameter estimation was performed in *gPROMS* software[34] providing the best fit of measured and predicted data using the maximum likelihood method.[35]

The objective function associated with the parameter estimation is described by the following equation:

$$\Phi = \frac{N}{2}\ln(2\pi) + \frac{1}{2}\min_{\theta}\left\{\sum_{i=1}^{NE}\sum_{j=1}^{NV_i}\sum_{k=1}^{NM_{i,j}}\left[\ln(\sigma_{ijk}^{\ 2}) + \frac{(\tilde{z}_{ijk} - z_{ijk})^2}{\sigma_{ijk}^{\ 2}}\right]\right\} \qquad (17)$$

where $\tilde{z}_{ijk}$ and z_{ijk} are the measured and predicted data, respectively, N is the total number of measurements taken during the experiments, θ is the set of parameters to be estimated (k_c and $K_{s,D}$), NE is the number of experiments performed, NV_i is the number of variables measured in the ith experiment, NM_{ij} is the number of measurements of the jth variable, and $\sigma_{ijk}^{\ 2}$ is the variance of the kth measurement of variable j in experiment i.

The results of the parameter estimation for different temperatures are presented in Table 2.

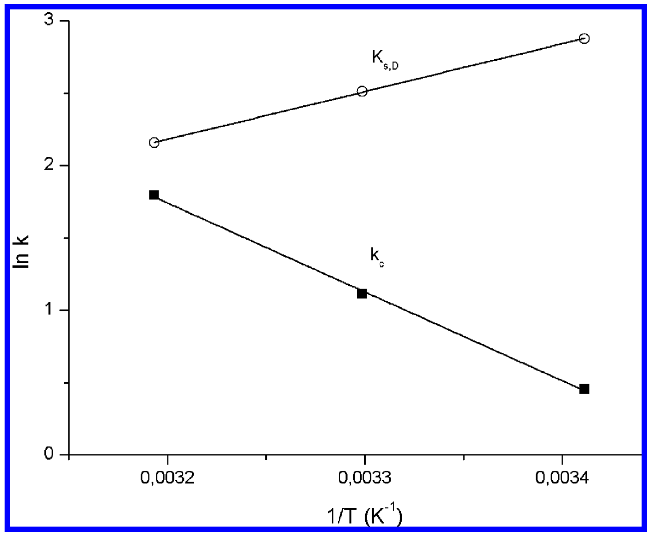

Figure 7. Representation of the experimental values of k_c and $K_{s,D}$ as a function of $1/T$ and linear fitting.

Table 3. Kinetic Law and Parameters Used in Batch Reactor Model Simulations

kinetic law	$\mathscr{R} = k_c[(a_A a_B - a_c a_d/K_a a_A)/(1 + K_{s,D} a_D)^2]$
equilibrium constant (dimensionless)	$K_a = 9.59 \times 10^{-3} \exp[1755.3/T \text{ (K)}]$
kinetic constant (mol g_{cat}^{-1} min^{-1})	$K_c = 2.39 \times 10^9 \exp[-6200.9/T \text{ (K)}]$
water adsorption constant (dimensionless)	$K_{s,D} = 2.25 \times 10^{-4} \exp[3303.1/T \text{ (K)}]$

The temperature dependence of the estimated parameters is given by the Arrhenius equation:

$$k_c = k_{0,c}\exp\left(-\frac{E_{a,c}}{RT}\right) \qquad (18)$$

$$k_{s,D} = k_{0,s}\exp\left(-\frac{\Delta H_s}{RT}\right) \qquad (19)$$

The predicted values of k_c and $K_{s,D}$ are represented as a function of the temperature in Figure 7. By fitting of the predicted values by eq 18 and eq 19, $E_{a,c} = 51.55$ kJ mol^{-1} and $\Delta H_s = -27.5$ kJ mol^{-1} are obtained.

7. Model Results

The kinetic law and the parameters of the batch reactor model considered in the following simulations are presented in Table 3.

Parts a and b of Figure 8 show the time evolution of the amount (moles) of reactants (butanol and acetaldehyde) and products (acetal DBE and water) at two different temperatures (293.15 and 313.15 K); a comparison between the experimental and simulated results is also presented.

In order to validate the estimation of the mass-transfer parameters, experiments for different particle diameters were performed. Parts a and b of Figure 9 show that the model gives a good prediction of the batch reaction for both experiments and, therefore, the good agreement between the experimental and simulated results leads us to conclude that the model gives a good prediction of the effect of the internal mass-transfer resistance.

By simulation, it is possible to observe the effect of the particle diameter on the internal concentration profile. Figure 10 shows the internal concentration profile of butanol for

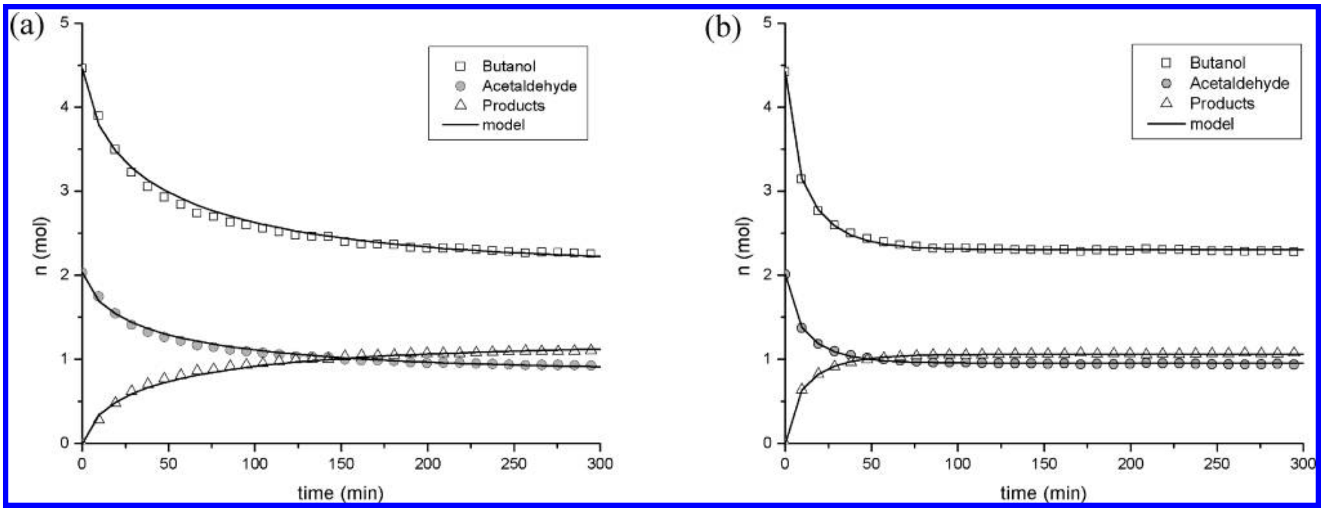

Figure 8. Experimental and simulated kinetic curves: $P = 6$ atm, $w_{cat} = 1.8$ g, $d_p = 0.550$ mm, and $r_{A/B} = 2.2$ for (a) 293.15 K and (b) 313.15 K.

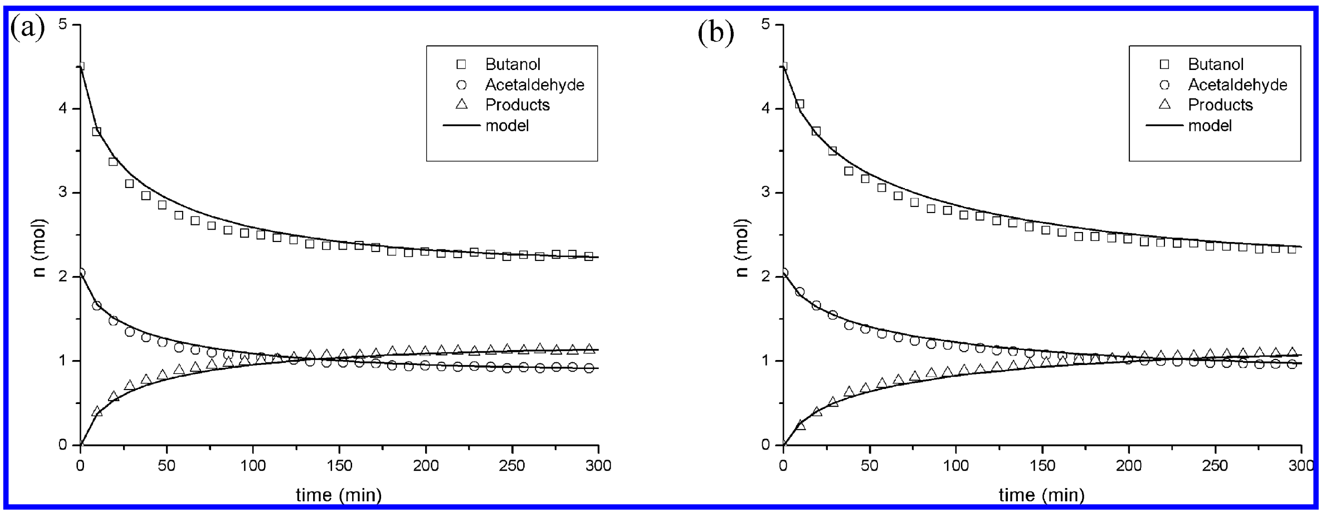

Figure 9. Experimental and simulated kinetic curves: $T = 293.15$ K, $P = 6$ atm, $w_{cat} = 1.8$ g, $r_{A/B} = 2.2$ for (a) $d_p = 0.428$ mm and (b) $d_p = 0.890$ mm.

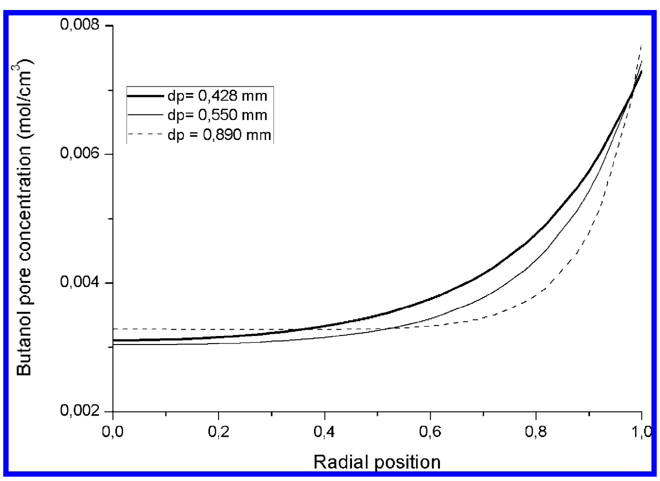

Figure 10. Internal concentration profile of butanol for $t = 9.5$ min.

three particle diameters. The presence of a concentration gradient between the surface and the center of the catalyst indicates the presence on the internal mass-transfer resistances. The internal concentration profile is more abrupt for greater particle diameter, indicating that the internal mass-transfer resistance increases with the particle diameter, as was expected.

In order to evaluate how much the internal mass transfer is controlling the kinetic experiments, it is possible to calculate the catalyst effectiveness factor for each experiment, which is defined by the following expression:

$$\eta = \frac{\langle \mathscr{R} \rangle}{\mathscr{R}_s} = 3\frac{\int_0^1 \rho^2 \mathscr{R}\, d\rho}{\mathscr{R}_s} \tag{20}$$

where $\mathscr{R}_s$ is the reaction rate at surface conditions and $\langle \mathscr{R} \rangle$ is the average reaction rate defined as

$$\langle \mathscr{R} \rangle = \frac{\int_0^{r_p} r^2 \mathscr{R}\, dr}{\int_0^{r_p} r^2\, dr} = 3\int_0^1 \rho^2 \mathscr{R}\, d\rho \tag{21}$$

The highest effectiveness factor of about 69% at equilibrium was obtained using a catalyst with an average diameter of 428 μm (Figure 11). For the largest particle diameter of 890 μm, the effectiveness factor is about 42% at equilibrium. From this, it is possible to conclude that all experiments were performed under a diffusion-controlled regime. In order to

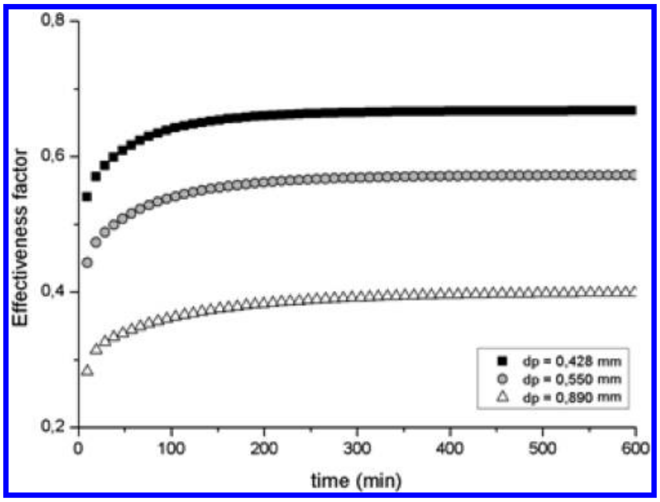

Figure 11. Effectiveness factor time evolution.

Table 4. Acetalization Reaction of Acetaldehyde with Methanol (Reaction 1), Ethanol (Reaction 2), and 1-Butanol (Reaction 3)[a]

	X_{eq}	$t_{1/2}$ (min)	η	$E_{a,c}$ (kJ mol^{-1})
reaction 1	0.63	40	0.16	72.4
reaction 2	0.56	180	0.36	65.1
reaction 3	0.53	764	0.61	51.6

[a] $P = 6$ atm, $w_{cat} = 0.5$ g, $d_p = 0.550$ mm, $r_{A/B} = 2$, and $T = 293.15$ K.

operate under a chemical reaction-controlled regime (effectiveness factor of about 1), it would be necessary to use a particle diameter of lower than 175 μm, which is not commercially available, and it is not possible to grind the resin without affecting its catalytic properties.[36]

In Table 4, acetalization reactions of acetaldehyde with methanol,[21] ethanol,[37] and 1-butanol are compared with the terms of equilibrium conversion, reaction half-life, effectiveness factors, and activation energy. These results show that both the equilibrium conversion and reaction rate decrease with an increase in the chain length of the alcohol.

8. Conclusions

The DBE synthesis in a liquid-phase reaction catalyzed by Amberlyst-15 was studied in a laboratory-scale batch reactor. The thermodynamic equilibrium constant was calculated based on the equilibrium compositions in the temperature range of 293.15−323.15 K and is given by the expression $K_a = 0.00959 \exp[1755.3/T\ (\mathrm{K})]$. The reaction is exothermic, and the standard properties of the reaction at 298.15 K are $\Delta H° = -14\,593.6$ J mol^{-1}, $\Delta S° = -38.6$ J mol^{-1} K^{-1}, and $\Delta G° = -3074.1$ J mol^{-1}.

Kinetic experiments showed that the rate of reaction increases with the temperature; however, the equilibrium conversion decreases with the temperature because of the exothermic nature of the reaction. Experiments performed at different particle diameters showed the existence of internal mass-transfer resistances for particle diameters greater than 0.5 mm.

Because of the strong nonideality of the liquid reaction mixture, both the equilibrium constant and kinetic law were expressed in terms of activities. The activation energy of 51.55 kJ mol^{-1} was calculated by fitting the estimated kinetic parameters at different temperatures to the Arrhenius equation.

A comparison between the experimental and simulated results shows that the model gives a good representation of the batch reactor performance for different temperatures and particle diameters of the catalyst. The simulated results of the catalyst internal concentration profiles showed a concentration gradient between the surface and the center of catalyst because of the presence of internal mass-transfer resistances. The time evolution of the effectiveness factor, for different particle diameters, shows that the controlling mechanism is the internal diffusion.

This work is an important step for further implementation of an integrated reaction−separation process, such as a SMBR, in order to enhance the conversion of the reaction limited by chemical equilibrium.

Acknowledgment

N.S.G. acknowledges Fundação para a Ciência e a Tecnologia for the Ph.D. Research Fellowship SFRH/BD/41107/2007.

Appendix A. UNIFAC Method Parameters

Tables A1 and A2 present the UNIFAC method parameters used in this work to calculate the activity coefficients (γ_i).

Table A1. Relative Molecular Volume and Surface Parameters of a Pure Species[38]

	group identification					
molecule i	name	no. of main groups	no. of secondary groups	$\upsilon_k^{(i)}$	R_k	Q_k
1-butanol	CH_3	1	1	1	0.9011	0.848
	CH_2	1	2	3	0.6744	0.540
	OH	5	15	1	1.0000	1.200
acetaldehyde	CH_3	1	1	1	0.9011	0.848
	CHO	10	21	1	0.9980	0.948
DBE	CH_3	1	1	3	0.9011	0.848
	CH_2	1	2	4	0.6744	0.540
	CH	1	3	1	0.4469	0.228
	CH_2O	13	26	2	0.9183	0.780
water	H_2O	7	17	1	0.8200	1.400

Table A2. Interaction Parameters[28]

$a_{m,n}$	1	5	7	10	13
1	0	986.5	1318	677	251.5
5	156.4	0	353.5	−203.6	28.06
7	300	−229.1	0	−116	540.5
10	505.7	529	480.8	0	304.1
13	83.36	237.7	−314.7	−7.838	0

Table A3. Pure-Component Liquid Molar Volume and Viscosity for Different Temperatures[45]

	liquid molar volume (mL mol^{-1})				viscosity (cP)			
T (K)	V_A	V_B	V_C	V_D	η_A	η_B	η_C	η_D
293.15	91.57	56.48	208.51	18.05	2.899	0.228	1.183	0.996
303.15	92.42	57.45	213.15	18.09	2.249	0.223	0.988	0.787
313.15	93.31	58.48	217.79	18.16	1.780	0.220	0.820	0.645
323.15	94.24	59.60	222.43	18.23	1.411	0.214	0.679	0.544

Table A4. Liquid Mixture Viscosity and Molecular Diffusivities Calculated Based on the Equilibrium Composition (Table 1)

		molecular diffusivity (cm^2 s^{-1}) × 10^5			
T (K)	liquid mixture viscosity η_m (cP)	$D_{A,m}$	$D_{B,m}$	$D_{C,m}$	$D_{D,m}$
293.15	0.923	1.654	2.191	0.490	6.930
303.15	0.796	1.994	2.704	0.566	8.538
313.15	0.695	2.386	3.321	0.639	10.468
323.15	0.601	2.871	4.060	0.736	12.844

Appendix B. Effective Diffusivity Calculation

The effective diffusivity D_j of the compound j is given by

$$D_j = \frac{\varepsilon_p D_{j,m}}{\tau} \quad (22)$$

where $D_{j,m}$ is the molecular diffusivity of compound j in the multicomponent mixture and τ is the tortuosity of an ion-exchange resin. The coefficients $D_{j,m}$ were estimated in a way similar to that performed to the system of ethyl lactate synthesis; once one reactant (lactic acid solution) has a high viscosity, similarly to this case, where butanol is very viscous also.[30] Different values of τ_p, such as 1.3,[39] 2,[40] and 4.9,[41] are reported in the literature for calculation of the effective diffusivity in Amberlyst-15. Estimations of the tortuosity were made using the correlations given by Wakao and Smith[42] ($\tau_p = 1/\varepsilon_p$) and Suzuki and Smith[43] [$\tau_p = \varepsilon_p + 1.5(1 - \varepsilon_p)$]; the values obtained with $\varepsilon_p = 0.36$ were 2.78 and 1.32, respectively. In this work, the tortuosity used was 2, i.e., the mean between the estimated values.

The infinite dilution molecular diffusivities were estimated by the Scheibel correlation, which modified the Wilke−Chang equation in order to eliminate its association factor:[44]

$$D^0_{j,i} = \frac{8.2 \times 10^{-8}}{\eta_i V_j^{1/3}}\left[1 + \left(\frac{3V_i}{V_j}\right)^{2/3}\right] \quad (23)$$

where $D^0_{j,i}$ is the diffusion coefficient for a dilute solute j in a solvent i,V_j is the molar volume of the component j, and η_i is the viscosity of solvent i. Table A3 presents the liquid molar volume and viscosity for the pure components.

For a concentrated multicomponent system, the Perkins and Geankoplis[46] method was used:

$$D_{j,m}\eta_m^{\ 0.8} = \sum_{\substack{i=1 \\ i\neq j}}^{n} x_i D^0_{j,i}\eta_i^{\ 0.8} \quad (24)$$

The viscosity of the liquid mixture was calculated by the Grunberg−Nissan approach:[47]

$$\ln(\eta_m) = x_1 \ln(\eta_1) + x_2 \ln(\eta_2) + x_1 x_2 G_{1,2} \quad (25)$$

where $G_{1,2}$ is an empirical interaction parameter adjusted by the experimental data. The liquid mixture viscosity and the molar diffusivities are presented in Table A4.

Appendix C

Notation

a = liquid-phase activity
A_p = external exchange area between the bulk and the particles
C_i = concentration, mol cm^{-3}
C_b = bulk concentration, mol cm^{-3}
C_p = concentration inside the particle, mol min^{-3}
d_p = average particle diameter, mm
D_j = effective diffusivity, cm^2 min^{-1}
$D_{j,m}$ = molecular diffusivity coefficient of a solute in a mixture, cm^2 min^{-1}
$E_{a,c}$ = reaction activation energy, kJ mol^{-1}
$\Delta G°$ = standard Gibbs free energy, J mol^{-1}
$\Delta H°$ = standard enthalpy, J mol^{-1}
ΔH_s = enthalpy of adsorption, J mol^{-1}
k_c = kinetic constant, mol g_{cat}^{-1} min
$k_{0,c}$ = Arrhenius constant for eq 18, mol g_{cat}^{-1} min
$k_{0,s}$ = Arrhenius constant for eq 19, mol g_{cat}^{-1} min
K_a = equilibrium constant based on activities
K_x = equilibrium constant based on the molar fraction
K_γ = equilibrium constant based on activity coefficients
K_s = equilibrium adsorption constant
n = number of moles, mol
P = pressure, atm
R = gas constant, J mol^{-1} K^{-1}
r = radial position, cm
r_p = particle radius, mm
$r_{A/B}$ = initial molar ratio of the reactants
$\Delta S°$ = standard entropy, J mol^{-1} K^{-1}
$\mathcal{R}$ = reaction rate, mol g_{cat}^{-1} min
$\mathcal{R}_s$ = reaction rate at surface conditions, mol g_{cat}^{-1} min
$\langle\mathcal{R}\rangle$ = average reaction rate, mol g_{cat}^{-1} min
$\mathcal{R}^p$ = reaction rate relative to the local pore concentration, mol g_{cat}^{-1} min
t = time coordinate, min
T = temperature, K
x = molar fraction
X = conversion of the limiting reactant
V = volume of the solution, cm^3
V_{liq} = total volume of the reactant mixture, cm^3
V_p = total volume of the particles, cm^3
w_{cat} = mass of the dry catalyst, g

Greek Letters

γ = activity coefficient
ε_b = bulk porosity
ε_p = particle porosity
η = effectiveness factor
ρ = dimensionless radial coordinate
ρ_p = particle density, g cm^{-3}
υ = stoichiometric coefficient
τ_p = tortuosity factor

Subscripts

A = butanol
B = acetaldehyde
C = DBE
D = water
i = relative to component i
liq = liquid phase
p = relative to the particle
s = relative to the surface of the particle

Literature Cited

(1) Wen, L. B.; Xin, C. H.; Yang, S. C. *Effect of adding dimethyl carbonate (DMC) and ethanol to unleaded gasoline on exhaust emission*. Published online, July 17, 2009, by Elsevier.

(2) Miyamoto, N.; Ogawa, H.; Obata, R.; Arima, T. *Smokeless, Low Nox, High thermal efficiency, and low noise diesel combustion with oxygenated agents as main fuel*; Publication SAE-98506; Society of Automotive Engineers: Washington, DC, 1998.

(3) Li, T.; Suzuki, M.; Ogawa, H. Effects of ethyl *tert*-butyl ether addiction to diesel fuel on characteristics of combustion and exhaust emissions of diesel engines. *Fuel* **2009**, *88*, 2017–2024.

(4) Naegeli, D.; Dodge, L. *Combustion Characterization of Methylal in Reciprocating Engines*. Final Report No. SwRI 03-130; Southwest Research Institute: San Antonio, TX, 1992.

(5) Frusteri, F.; Spadaro, L.; Beatrice, C.; Guido, C. Oxygenated additives production for diesel engine emission improvement. *Chem. Eng. J.* **2007**, *134*, 239–245.

(6) Iwasaky, H.; Kitayama, M.; Onishi, T. Process for producing acetals. U.S. Patent 5,792,876, 1998.

(7) Kohlpaintner, C.; Schulte, M.; Falbe, J.; Lappe, P.; Weber, J. Aldehydes, Aliphatic and Araliphatic. *Ullmann's Encyclopedia of Industrial Chemistry*; Wiley-VCH: Weinheim, Germany; 1999 (electronic release).

(8) Yadav, G. D.; Pujari, A. A. Kinetics of acetalization of perfumery aldehydes with alkanols over solid acid catalysts. *Can. J. Chem. Eng.* **1999**, *77*, 489–496.

(9) Hille, M. L.; Weinelt, F. B.; Wittikus, H.; Reimann, W. Environmentally friendly diesel fuel. U.S. Patent 6,013,114, 2000.

(10) Egwaw, T.; Kawaguchi Y.; Mogami, K.; Shimizu N. Method of producing a polyvinyl ether compound. U.S. Patent 5,616,812, 1997.

(11) Weizmann, C. Process for carrying out condensation reactions. U.S. Patent 2,474,175, 1949.

(12) Guinot, H. M. Process for the Manufacture of Acetal. U.S. Patent 1,850,836, 1932.

(13) Silva, V. M. T. M.; Rodrigues, A. E. Synthesis of diethylacetal: thermodynamics and kinetic studies. *Chem. Eng. Sci.* **2001**, *56*, 1255–1263.

(14) Düre, P. Biobutanol: An alternative biofuel. *Biotchnol. J.* **2007**, *2*, 1525–1534.

(15) Kaufhold, M. M.; El-Chabawi, M. T. Process for Preparing Acetaldehyde Diethyl Acetal. U.S. Patent 5,527,969, 1996.

(16) Lilja, J.; Murzin, D. Y.; Salmi, T.; Aumo, J.; Mäki-Avela, P.; Sundell, M. Esterification of different acids over heterogeneous and homogeneous catalyst and correlation with Taft equation. *J. Mol. Catal. A: Chem.* **2002**, *182*−*183*, 555–563.

(17) Kolah, A. K.; Asthana, N. S.; Vu, D. T.; Lira, C. T.; Miller, D. J. Reaction kinetics of the catalytic esterification of citric acid with ethanol. *Ind. Eng. Chem. Res.* **2007**, *46*, 3180–3187.

(18) Andrade, J.; Arntz, D.; Prescher, G. Method for Preparation of Acetals. U.S. Patent 4,579,979, 1986.

(19) Capeletti, M. R.; Balzano, L.; de la Poente, G.; Laborde, M.; Sadran, U. Synthesis of acetal (1,1-diethoxyethane) from ethanol and acetaldehyde over acidic catalyst. *Appl. Catal., A* **2000**, *198*, L1–L4.

(20) Silva, V. T. M.; Rodrigues, A. E. A Novel Process for Diethylacetal Synthesis. *AIChE J.* **2005**, *51*, 2752–2768.

(21) Gandi, G. K.; Silva, V. M. T. M.; Rodrigues, A. E. Process development for the dimethylacetal synthesis: thermodynamics and kinetic studies. *Ind. Eng. Chem. Res.* **2005**, *44*, 7287–7297.

(22) Gandi, G. K.; Silva, V. M. T. M.; Rodrigues, A. E. Acetaldehyde dimethylacetal synthesis with Smopex 101 fibers as catalyst/adsorbent. *Chem. Eng. Sci.* **2007**, *62*, 907–918.

(23) Rat, M.; Zahedi-Niaki, M. H.; Kaliaguine, S.; Do, T. O. Sulfonic acid functionalized periodic mesoporous organosilicas as acetalization catalyst). *Microporous Mesopouros Mater.* **2008**, *112*, 26–31.

(24) Mahajani, S. M.; Kolah, A. K.; Sharma, M. M. Extractive reactions with cationic exchange resins catalysts (acetalization of aldehydes with alcohols). *React. Funct. Polym.* **1995**, *28*, 29–38.

(25) Blagova, S.; Parada, S.; Bailer, O.; Moritz, P.; Lam, D.; Weinand, R.; Hasse, H. Influence of ion-exchange resin catalyst on side reactions of the esterification of *n*-Butanol with acetic acid. *Chem. Eng. Sci.* **2006**, *61*, 753–765.

(26) Silva, V. M. T. M.; Gandi, G. K.; Rodrigues, A. E. Development of Simulated Moving Bed Reactor Using a Cation Exchange Resin as a Catalyst and Adsorbent for the Synthesis of Acetals. In *Ion Exchange and Solvent Extraction: A Series of Advances*; Sen Gupta, A. K., Ed.; CRC: Boca Raton, FL, 2007; Vol. 18.

(27) Sanz, M. T.; Murga, R.; Beltrán, S.; Cabezas, J. L.; Coca, J. Kinetic for the reactive system of lactic acid esterification with methanol: methyl lactate hydrolysis reaction. *Ind. Eng. Chem. Res.* **2004**, *43*, 2049–2053.

(28) Fredeslund, A.; Gmehling, J.; Rasmussen, P. *Vapor*−*liquid Equilibrium Using UNIFAC*; Elsevier: Amsterdam, The Netherlands, 1977.

(29) Xu, Z. P.; Chuang, K. T. Effect of internal diffusion on heterogeneous catalytic esterification of acetic acid. *Chem. Eng. Sci.* **1997**, *52*, 3011–3017.

(30) Pereira, C. S. M.; Silva, V. M. T. M.; Rodrigues, A. E. Fixed Bed Adsorptive Reactor for Ethyl Lactate Synthesis: Experiments, Modelling, and Simulation. *J. Sep. Sci.Technol.* **2009**, *44*, 2721–2749.

(31) Dogu, T.; Aydin, E.; Boz, N.; Murtezaoglu, K.; Dogu, G. Diffusion Resistances and Contribution of Surface Diffusion in TAME and TAEE Production Using Amberlyst-15. *Int. J. Chem. React. Eng.* **2003**, *1*, A6.

(32) Morrison, R.; Boyd, R. *Organic Chemistry*; Allyn and Bacon: Boston, 1983.

(33) Jermy, B. R.; Pandurangan, A. Al-MCM-41 as an efficient heterogeneous catalyst in the acetalization of cyclohexanone with methanol, ethylene glycol and pentaerythritol. *J. Mol. Catal. A: Chem.* **2006**, *256*, 184–192.

(34) *gPROMS. Advanced User Guide. Process Systems*; Enterprise Ltd.: London, 2002.

(35) Pereira, C. M.; Pinho, S. P.; Silva, V. M. T.; Rodrigues, A. E. Thermodynamic equilibrium and reaction kinetics for the esterification of lactic acid with ethanol catalyzed by acid ion exchange resin. *Ind. Eng. Chem. Res.* **2007**, *47*, 1453–1463.

(36) Pöpken, T.; Götze, L.; Gmehling, J. Reaction kinetics and chemical equilibrium of homogeneously and heterogeneously catalyzed acetic acid esterification with methanol and methyl acetate hydrolysis. *Ind. Eng. Chem. Res.* **2000**, *39*, 2601–2611.

(37) Silva, V. M. T. M.; Rodrigues, A. E. Kinetic Studies in a Batch Reactor using Ion-Exchange Resin Catalysts for Oxygenates Production: the Role of Mass Transfer Mechanisms. *Chem. Eng. Sci.* **2006**, *61*, 316–331.

(38) Reid, C. R.; Prausnitz, J. M.; Poling, B. E. *The Properties of Gases & Liquids*; McGraw-Hill: New York, 1987.

(39) Yu, W.; Hidajat, K.; Ray, A. K. Determination of Adsorption and Kinetic Parameters for Methyl Acetate Esterification and Hydrolysis Reaction Catalyzed by Amberlyst 15. *Appl. Catal., A* **2004**, *260*, 191–205.

(40) Silva, V. M. T. M. Diethylacetal synthesis in simulated moving bed reactor. Ph.D Thesis, University of Porto, Porto, Portugal, 2003.

(41) Oktar, N.; Mürtezauglu, K.; Dogu, T.; Dogu, G. Dynamic Analysis of Adsorption Equilibrium and Rate Parameters of Reactants and Products in MTBE, ETBE and TAME Production. *Can. J. Chem. Eng.* **1999**, *77*, 406–412.

(42) Wakao, N.; Smith, J. M. Diffusion in Catalyst Pellets. *Chem. Eng. Sci.* **1962**, *17*, 256–264.

(43) Suzuki, M.; Smith, J. M. Axial Dispersion in Beds of Small Particles. *Chem. Eng. J.* **1972**, *3*, 256–264.

(44) Scheibel, E. G. Liquid diffusivities, Viscosity of gases. *Ind. Eng. Chem.* **1954**, *46*, 2007–2009.

(45) Rowley, R. L.; Wilding, W. V.; Oscarson, J. L.; Zundel, N. A.; Marshall, T. L.; Daubert, T. E.; Danner, R. P. *DIPPR® Data Compilation of Pure Compound Properties*; Design Institute for Physical Properties, AIChE: New York, 2002.

(46) Perkins, L. R.; Geankopolis, C. J. Molecular diffusion in ternary liquid system with diffusing component dilute. *Chem. Eng. Sci.* **1969**, *24*, 1035–1042.

(47) Grunberg, L.; Nissan, A. H. Mixture law for viscosity. *Nature* **1949**, *164*, 799–800.

Received for review October 19, 2009
Revised manuscript received March 18, 2010
Accepted March 26, 2010

IE901635J